COMPARING UAV AND SATELLITES ACCURACY IN SIMULATING FINE-SCALE ALPINE GRASSLAND HETEROGENEITY IN PERIGLACIAL ENVIRONMENT

FENG, X.[1] – WEN, A. M.[2*] – LI, L.[1,3] – WU, T. H.[2] – YAN, S. W.[1]

[1]*Lanzhou Resources & Environment Voc-Tech University, Lanzhou 730021, China*

[2]*Cryosphere Research Station on the Qinghai-Tibet Plateau, State Key Laboratory of Cryospheric Science and Frozen Soil Engineering, Northwest Institute of Eco-Environment and Resources, Chinese Academy of Sciences, Lanzhou 730000, China*

[3]*College of Geographical and Environmental Science, Northwest Normal University, Lanzhou 730070, China*

**Corresponding author*
e-mail: wenamin@nieer.ac.cn; phone: +86-136-0930-1510

(Received 27th Jun 2025; accepted 1st Sep 2025)

Abstract. Coarse resolution imagery poses significant monitoring challenges in fragile alpine ecosystem. Thus, addressing underlying surface heterogeneity offers a promising approach to enhance the accuracy of alpine grassland characteristics retrieval. This study investigates the potential of fixed-wing unmanned aerial vehicle (UAV) for large-area monitoring of alpine grassland characteristics in high-altitude and low-temperature permafrost environments, where fine-scale heterogeneity poses challenges for traditional remote sensing techniques. By integrating multispectral imaging and Structure-from-Motion (SfM) photogrammetry, the vegetation index (VIs), fraction vegetation cover (FVC) and vegetation type maps were generated in the Wudaoliang region of the central Qinghai-Tibet Plateau (QTP). We also qualitatively compared the UAV-based vegetation information at sub-meter spatial resolution with that provided by satellites (including Sentinel-2, Landsat-8 and MODIS) at coarser resolutions. The results show that, compared with the other four VIs, including Kernel Normalized Difference Vegetation Index (kNDVI), Enhanced Vegetation Index (EVI), Soil-Adjusted Vegetation Index (SAVI) and Excess Green Index (ExG), the calibrated UAV-based Normalized Difference Vegetation Index (NDVI) achieved the best accuracy for alpine grassland FVC estimation, significantly outperforming in detecting low-stature alpine grassland. UAV imagery unveiled pronounced fine-scale heterogeneity in both FVC and alpine grassland types, strongly correlated with periglacial landforms and microtopography, while these patterns are largely invisible to satellites. Satellites data underestimates the spatial heterogeneity within alpine grasslands, which may lead to inadequate monitoring of fine-scale ecological variations. Our results provide a detailed assessment of spatial heterogeneity within alpine grassland in high-altitude periglacial environments, which offers valuable insights for ecological models predicting alpine variation and permafrost stability feedback.
Keywords: *alpine grassland mapping, spatial heterogeneity, unmanned aerial vehicle (UAV), periglacial environment, Qinghai-Tibet Plateau*

Introduction

The Qinghai-Tibet Plateau (QTP), dominated by alpine grasslands (>70% coverage) (Wang et al., 2016), serves as a critical regulator of permafrost stability, carbon cycling, and regional climate feedbacks (Piao et al., 2015; Mu et al., 2020). QTP is undergoing the twice climate warming rate of the global average during the past few decades (Biskaborn et al., 2019; Zhu et al., 2024). The accelerated warming has triggered widespread permafrost degradation and thaw-induced subsidence, driving complex vegetation-topography interactions that amplify landscape heterogeneity (Peng et al.,

http://www.aloki.hu ● ISSN 1589 1623 (Print) ● ISSN 1785 0037 (Online)
DOI: http://dx.doi.org/10.15666/aeer/2305_1029310313

2020; Heijmans et al., 2022). This spatial variability fundamentally alters hydrothermal processes, snow dynamics, and ecosystem responses to climate change (Nitzbon et al., 2024; Liljedahl et al., 2024), yet current understanding remains constrained by observational limitations across scales. While satellite remote sensing enables regional vegetation monitoring (Yang et al., 2024; Zhou et al., 2025), coarse resolutions of satellites (250 m – 1 km) fails to resolve meter-scale heterogeneity critical for permafrost-vegetation coupling, creating systematic biases in ecosystem models.

Several studies have reported that alpine grassland ecosystems on the QTP exhibit high spatial and temporal complexity in land covers and surface landscapes (Li et al., 2020). Vegetation indices (VIs)—particularly Normalized Difference Vegetation Index (NDVI), Enhanced Vegetation Index (EVI), and Kernel Normalized Difference Vegetation Index (kNDVI)—are widely used to estimate vegetation properties and variations (Ge et al., 2018; Marcial-Pablo et al., 2021; Duan et al., 2024). However, the performance of VIs degrades in heterogeneous alpine environments due to mixed-pixel effects and scale mismatches between field measurements (sub-meter) and satellite pixels (10–100 m) (Wang et al., 2021a; Zhong et al., 2023). Although Unmanned Aerial Vehicles (UAV) address this gap by providing centimeter-scale data, rotary-wing platforms face operational constraints in high-altitude permafrost zones, including limited coverage (<5 km^2) and flight endurance (Luo et al., 2021; Yi et al., 2021; Zhang et al., 2022). Fixed-wing UAVs offer superior efficiency for landscape-scale monitoring but require rigorous validation of spectral data consistency and operational reliability under extreme QTP conditions.

Recent advances in UAV-based multispectral sensors demonstrate promise for bridging observational scales. Fixed-wing systems enable efficient acquisition of high-resolution (10–50 cm) imagery across thermokarst-affected terrains while maintaining compatibility with satellite data fusion (Lou, 2022; Luo et al., 2020; Wen et al., 2025). Despite progress, three critical barriers persist: (1) insufficient protocols for scaling plot-level UAV data to ecosystem models (Assmann et al., 2020). The combination of UAV-derived data with satellite imagery offers the potential for more comprehensive and frequent monitoring, which is particularly important in remote or difficult-to-access areas (Chen et al., 2024). (2) unresolved uncertainties in VIs selection for heterogeneous vegetation mapping, and (3) limited integration of spectral metrics with permafrost degradation indicators, hindering the capacity to connect vegetation productivity and community with permafrost changes (Jin et al., 2021). Current studies predominantly focus on rotary-wing platforms or small-scale validation, leaving landscape-scale monitoring capabilities underdeveloped. This gap underscores the need for the development of standardized methodologies and better integration of UAV data with existing remote sensing technologies to enhance our ability to monitor large-scale environmental processes such as permafrost thaw and ecosystems shifts.

Despite technological advancements, limited validation of fixed-wing UAVs' operational efficiency and data consistency in high-altitude, low-temperature environments. This study aims to address these gaps by developing a fixed-wing UAV multispectral framework tailored for alpine permafrost zones, combining high-resolution vegetation mapping. The objectives of this paper are fourfold: (1) to quantify the accuracy and scalability of UAV-derived spectral reflectance against ground truth data; (2) to determine the best suitable vegetation indices for FVC estimation on the heterogeneous alpine grassland; (3) to compare the heterogeneous pattern of alpine grassland revealed by UAV and satellite imagery.

http://www.aloki.hu ● ISSN 1589 1623 (Print) ● ISSN 1785 0037 (Online)
DOI: http://dx.doi.org/10.15666/aeer/2305_1029310313

Materials and methods

Study area

The site is located at the Wudaoliang (WDL) basin (93°5′12.982″ E; 35°10′22.888″ N) on the QTP (*Fig. 1*). The study area is the typical permafrost regions and consists of mixed alpine grassland types and micro-topography. A national weather station, located in the northern study area, continuously records weather conditions for further atmospheric correction of UAV images and satellite data. Additionally, a portable automatic weather station was also installed in the flight site to record the weather conditions. The climate of WDL is with -4.82℃ annual mean air temperature and 314.3 mm annual precipitation. The observation also show that the annual mean air temperature and annual precipitation showed a significant increasing trend, with a rate of 5.3℃ per decade and 29.7 mm per decade. Permafrost degradation continues with a rate of 0.54℃ per decade. Annual precipitation also showed a significant increasing trend with a rate of 29.7 mm per decade. Thereby, the vegetation continues decreasing. The site for the experiments is chosen because: i) it offers diversity in terms of alpine grassland types and micro-topography; ii) it has easy access for UAV flight and field survey with convenient transport; iii) it allowed large enough to be imaged by several satellite pixels and revival; most importantly, iv) it is the typical and traditional regions for alpine grassland and permafrost monitoring on the QTP, and is large enough to be repeated by land surface models.

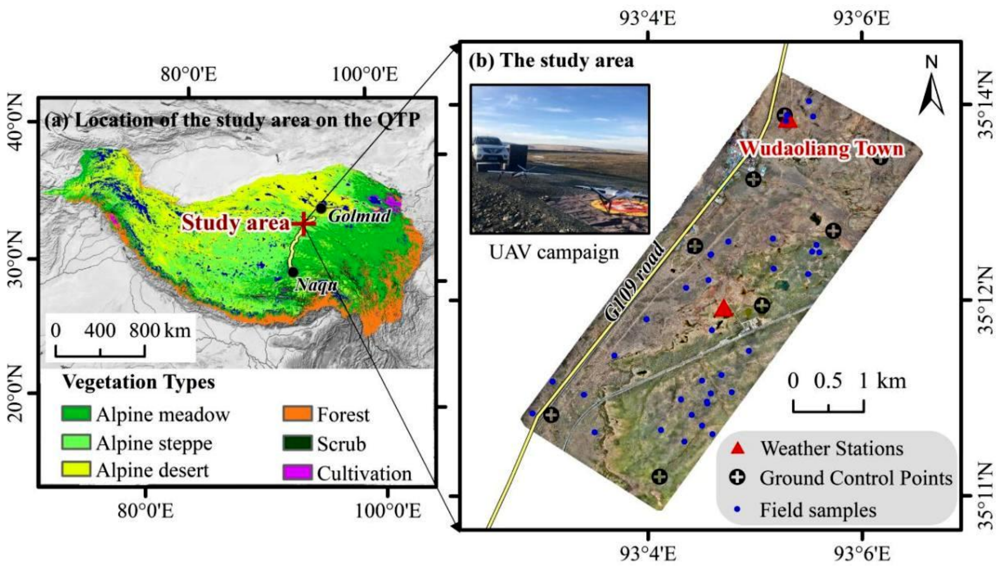

***Figure 1.** The study area, UAV systems and the distribution of field measurements. The vegetation type map on the Qinghai-Tibet Plateau (QTP) was download from Zhou et al. (2025)*

Field sampling

To ensure that the UAV-derived data is accurate, synchronizing the UAV flight campaign in April and August 2021, field experiments were conducted for validating the performance of the UAV-based VIs, FVC estimation and vegetation types classification. A handheld non-contact FieldSpec spectroradiometers (ASD, USA) was used for ground-measured reflectance measurements in the spectral range of 325–

http://www.aloki.hu ● ISSN 1589 1623 (Print) ● ISSN 1785 0037 (Online)
DOI: http://dx.doi.org/10.15666/aeer/2305_1029310313

1075 nm. A total of 16 typical surface points with relative uniform ground surface were measured vertically downward at 1 m above the ground. In order to improve the accuracy of measurements, each ground point was repeatedly measured (ten times), and then the average value was taken. Moreover, the geographic coordinates of the field samples were also been measured by the RTK to match them with UAV imagery. Finally, these in situ spectral reflectance data were resampled to match the band widths of the multi-spectral camera. By providing ground-measured reflectance, ASD measurements provide an additional vegetated ground calibration and validation target for the UAV multi-spectral images.

The in situ FVC were measured at 45 field plots using a digital camera (Cannon EOS R6, Canon Inc., Tokyo, Japan). The sampling sites were selected for using a uniform sampling methods. We calculate the observed FVC using the threshold-based photographic method (Kim et al., 2019). The field sites covered the entire study area and were highly variable over a very short distance. Each plot was 1 × 1 m (with the boundary delineated by white rope), which was consistent with mean FVC of 5 × 5 grid pixel for UAV. The coordinates of the four angular of each plot were also measured by Real-time kinematic (RTK). The spatial auto-correlation (Morans I) was examined based on the FVC sites. Additional, we investigated the vegetation types in these 45 field samples for identifying the vegetation types. According to the classification system proposed by Wang et al. (2016), the land cover types of the study area were classified as alpine meadow, alpine steppe, alpine desert, and others (*Fig. 2*). All of these sites, the 70% samples was used as the training data, and random distributed 30% samples was used for testing data in vegetation classification.

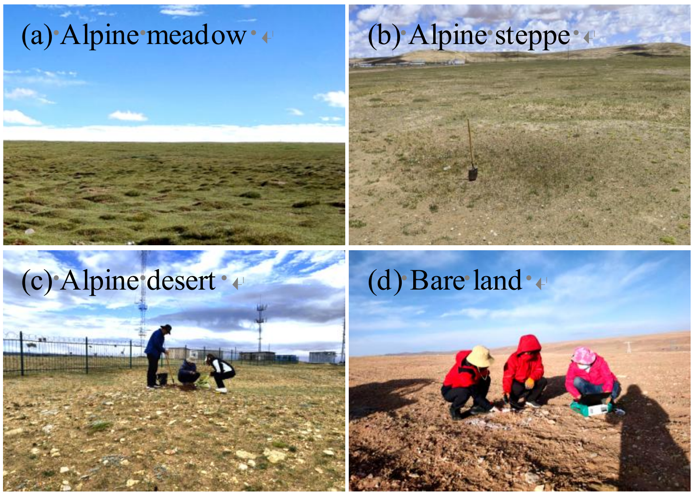

Figure 2. *Different land cover types of the study area:(a) alpine meadow, (b) alpine steppe, (c) alpine desert, and (d) bare land*

Moreover, before starting the flights, eight ground control points (GCPs) panels measured with a KOLIDA RTK differential GNSS device (KOLIDA Instrument Co., Ltd., Guangzhou, Guangdong, China) with about 1 cm accuracy, were arranged uniformly on the ground and used to improve vertical and horizontal accuracy of the output Digital Elevation Model (DEM) and orthomosaicss. Moreover, due to the cloudy and changeable weather of WDL, a rigorous atmospheric correction was necessary to obtain accurate and interpretable data. Thus, in order to obtain ground reflectance

http://www.aloki.hu ● ISSN 1589 1623 (Print) ● ISSN 1785 0037 (Online)
DOI: http://dx.doi.org/10.15666/aeer/2305_1029310313

calibration data, four custom-designed black, grey, white and aluminum calibration panels (1 × 1 m) were positioned on the ground to radiometric calibration and geometric correction of multi-spectral images. The basic radiometric calibration was conducted using the irradiance values captured by the sun-shine sensor during the flight and calibrated reflectance panel before and after the flight.

UAV data collection and image pre-processing

We performed the UAV campaigns using a FEIMA V300 (Feima Robotics Co. Ltd., Shengzhen, China) fixed-wing mapping drone. The UAV surveys covered 27 km^2 and conducted both in April (the cold season) and August (the warm season) 2021. Two cameras were equipped on the UAV platform to captured the high-resolution visible and multi-spectral images. The first camera was a Sony DSC-RX1RM2 digital RGB equipped with a 35 mm focal length lens and acquiring 7952 × 5304 pixel images. The second camera was the Micasense RedEdge-M (MicaSense, Inc., Seattle, WA, USA) multispectral sensor, which has a 6 mm focal length lens and acquiring 1280 × 960 pixel images. All missions were planned at a flight height of 200 m, a flight speed of 4–8 $m \cdot s^{-1}$ with a front overlaps of 85% and a side overlap of 80%. The Micasense RedEdge-M camera is composed of five individual camera with spectral resolution of Blue band (475 nm center, 20 nm bandwidth), Green band (560 nm center, 20 nm bandwidth), Red band (668 nm center, 10 nm bandwidth), Red Edge band (717 nm center, 10 nm bandwidth), and NIR band (840 nm center, 40 nm bandwidth).

Pix4D mapper software (Pix4D SA, Lausanne, Switzerland) was employed to orthorectify and mosaic the UAV images. Processing of the UAV imagery was completed using the Structure from Motion (SfM) workflow as implemented in Pix4D software. Finally, the 5 cm spatial resolution True Digital Orthophoto Map (TDOM) images and Digital Elevation Model (DEM) data were generated from visible camera. The raw multi-spectral images with 18 cm spatial resolution were processed by camera and radiometric calibration, and then were converted to reflectance. Moreover, the MODTRAN radiative transfer model was used for the further atmospheric correction of multispectral imagery (MS) using the MODTRAN5.2.2 code. In order to further improve the spectral accuracy of the atmospheric corrected multi-spectral images, we performed a empirical line calibration, which is a method based on linear regression between ground-measured surface reflectance and UAV-based spectral reflectance (Holman et al., 2019).

Satellite data and preprocessing

Three different satellite data with the similar acquisition time of UAV were downloaded for revival NDVI and compare with UAV-based NDVI images (*Table 1*), including MODIS NDVI (earthexplorer.usgs.gov), Sentinel-2A MSI (scihub.copernicus.eu), and Landsat–8 OLI (earthexplorer.usgs.gov). The MODIS NDVI (250 m spatial resolution) is atmosphere-corrected and calculated as the normalized difference between bands1 (841–876 nm) and band2 (620–670 nm). The Sentinel-2 imagery had been preprocessed with ortho-rectification and geometric corrections at sub-pixel accuracy. Therefore, we perform radiometric calibration and atmospheric correction using Sen2Cor, and then resample all bands to 10 m resolution (2, 3, 4 and 8) by SNAP. Finally, Sentinel-2 based NDVI was calculated as the

http://www.aloki.hu ● ISSN 1589 1623 (Print) ● ISSN 1785 0037 (Online)
DOI: http://dx.doi.org/10.15666/aeer/2305_1029310313

normalized difference between band 8 (784.5–899.5 nm) and band 4 (650–680 nm). Landsat-8 OLI imagery (cloud > 50%) was preprocessed by geometric correction with RMSE < 0.5 pixel based on GCPs and atmospheric correction with FLASSH algorithm. The Landsat-8 NDVI (30 m resolution) was calculated as the normalized difference between band 5 (845–885 nm) and band 4 (630–680 nm). All above satellite images were adjusting by georeferencing to make match ground-control points to minimize geometric mismatches between satellite and UAV.

Table 1. *Summary of information regarding the UAV and satellite data used in this study. To ensure a consistent acquisition time for all satellite data and UAV campaigns, the period from 2021.8.08 to 2021.8.17 was selected for all satellite data*

Sensors	Data	Cloud cover	Spatial resolution	Date of data acquisition	Data source
UAV	DEM, TDOM, MS	0%	0.18 m	2021.8.13	This paper
Sentinel-2	MS	5%	10 m	2021.8.17	https://scihub.copernicus.eu/
Landsat-8	MS	15%	30 m	2021.8.08	https://earthexplorer.usgs.gov/
MODIS	NDVI	—	230 m	2021.8.13	https://search.earthdata.nasa.gov/

TDOM: True Digital Orthophoto Map images; DEM: Digital Elevation Model; MS: multispectral imagery; NDVI: Normalized Difference Vegetation Index (NDVI)

Vegetation characteristics retrieval

Five typical VIs, including NDVI, kNDVI, EVI, SAVI and ExG, which have a high correlation with FVC, were selected in this study (*Table 2*).

Table 2. *Calculation of vegetation index (VIs) and faction vegetation cover (FVC) from the visible and multi-spectral imagery*

Indices	Equations	Cites
NDVI	NDVI = (NIR – R) / (NIR + R)	Pettorelli et al. (2005)
kNDVI	kNDVI = tanh (NDVI^2)	Camps-Valls et al. (2021)
EVI	EVI = 2.5 × (NIR – R) / (NIR + 6 × R – 7.5 × B + 1)	Huete (2002)
SAVI	SAVI = (1 + L_1) × (NIR – R) / (NIR + R + L_1)	Huete (2002)
ExG	ExG = 2 × g – r – b	Woebbecke et al. (1995)

In the ExG vegetation index, the variants of r, g, b are defined as: r = R/(R + G + B), g = G/(R + G + B), b = B/(R + G + B), where R, G, and B represent the red, green, and blue bands of RedEdge camera, respectively. L_1 is the soil adjustment factor, which are considered by Ren et al. (2018) to be the best value of 0.2 for the alpine grassland of QTP

Following calculation of these variables, the simplest two-endmember linear mixture model was used to calculate the FVC according to the following equation (Gutman and Ignatov, 1998; Mu et al., 2018):

$$FVC = \frac{V - V_S}{V_V - V_S} \quad \text{(Eq.1)}$$

where V refers to any vegetation indices. Vs and Vv are VI values in the area that completely covered by soil and vegetation, respectively. We define the values of Vs and Vv based on the 5% and 95% confidence internal of the cumulative frequency

http://www.aloki.hu ● ISSN 1589 1623 (Print) ● ISSN 1785 0037 (Online)
DOI: http://dx.doi.org/10.15666/aeer/2305_1029310313

distribution of VI maps by R package. Moreover, considering both the computing efficiency and classification accuracy, the support vector machine (SVM) algorithms was used for the classification of land cover types based on 45 field samples.

Statistical analysis

Three statistical measurements, i.e., person correlation coefficient (R) and root-mean-squared error (RMSE), and mean bias error (MBE) were calculated using the following equations to validate the accuracy of estimation.

$$R = \frac{\sum_{i=1}^{n}(M_i - \overline{M})(O_i - \overline{O})}{\sum_{i=1}^{n}(M_i - \overline{M})^2(O_i - \overline{O})^2} \quad \text{(Eq.2)}$$

$$RMSE = \sqrt{\frac{\sum_{i=1}^{n}(M_i - O_i)^2}{n}} \quad \text{(Eq.3)}$$

$$MBE = \frac{\sum_{i=1}^{n}(M_i - O_i)}{n} \quad \text{(Eq.4)}$$

where n is the number of field plots, M_i represents the i_{th} UAV spectral reflectance estimate, O_i represents the i_{th} field measurements.

Results

Accuracy assessment of the calibrated UAV-based NDVI

Five bands of uncalibrated UAV MS camera show good fit with in situ measurements with R^2 was greater than 0.80, however, there were some slight biases. After calibration, the regression analysis results show that all five bands of UAV MS camera obtained more accurate reflectance value than that before calibration (*Fig. 3*). The mean R^2 increased from 0.80 to 0.92, the mean RMSE decreased from 0.05 to 0.03, and the MBE ranged from 0.02 to 0.00. The accuracy of UAV spectral reflectance was improved and the deviation was narrowed significantly. We demonstrated that the ground endearments of multiple targets in spectral reflectance correction effectively improved the quality of UAV spectral reflectance, which agreed well with the conclusion of Wang et al. (2021b).

Performance of UAV-based NDVI in FVC retrieval

Based on the calibrated spectral reflectance of UAV MS, five VIs, including NDVI, kNDVI, EVI, SAVI, and ExG, were then calculated. Subsequently, the FVC maps corresponding to five VIs was revealed and validated based on the in situ measurements (*Table 3*). The comparison results show that the correlation of NDVI with FVC was the highest ($R^2 = 0.980$ and RMSE = 4.45), followed by kNDVI (R = 0.978 and RMSE = 5.83), while ExG was the lowest (R = 0.855 and RMSE = 15.01%). The MBE values indicate that there is a slight underestimation for kNDVI, EVI, SAVI (MBE < 0), while a overestimation for NDVI and ExG (MBE > 0).

http://www.aloki.hu ● ISSN 1589 1623 (Print) ● ISSN 1785 0037 (Online)
DOI: http://dx.doi.org/10.15666/aeer/2305_1029310313

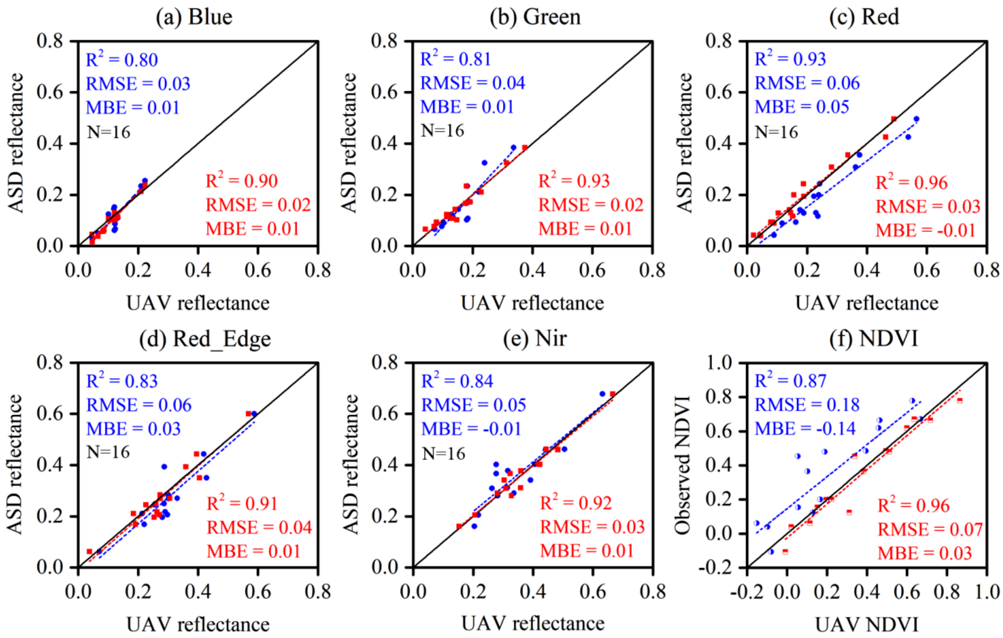

Figure 3. *Relationships between UAV estimations and in situ measurements for surface reflectance and fraction vegetation cover: (a) Blue band, (b) Green band, (c) Red band, (d) Red_edge band, (e) Nir band, and (f) fraction vegetation cover (FVC). The black line was the 1:1 line. During (a)–(e), the blue and red points represented the uncalibrated and calibrated UAV surface reflectance, and the red and blue dotted line are the fitting line*

Table 3. *Accuracy assessment for fraction vegetation cover (FVC) derived from five vegetation indices based on field measurements*

Statistical metrics	FVC				
	NDVI	**kNDVI**	**EVI**	**SAVI**	**ExG**
R^2	0.980	0.978	0.973	0.968	0.855
RMSE	4.45	5.83	5.97	8.56	15.01
MBE	1.11	-1.07	-2.12	-2.35	7.28

To further assess the ability of UAV-based VIs in revealing sub-grid vegetation patterns, we compared the superior two VIs: NDVI and kNDVI in different vegetation types linked to microtopography variations (*Fig. 4*). The results show that, spatially, in alpine meadow areas, NDVI and kNDVI have similar spatial patterns, both effectively detecting FVC. However, in alpine steppe and desert regions, kNDVI can only detect areas with higher FVC, while completely missing low-growing sparse vegetation. In contrast, NDVI performs well in detecting vegetation across all coverage types. The difference between NDVI and kNDVI (calculated as NDVI minus kNDVI) shows that NDVI values are consistently higher, with the largest differences occurring in areas with sparse and low-growing vegetation, which agree with the conclusions from Platel et al. (2025). Therefore, it is undoubtedly that NDVI is a more suitable and robust approach for FVC retrieval of vegetation in high altitude permafrost environment on the QTP. This robustness is critical given the prevalence of sparse vegetation across vast expanses of the plateau’s steppe and desert ecosystems, which are highly sensitive to

http://www.aloki.hu ● ISSN 1589 1623 (Print) ● ISSN 1785 0037 (Online)
DOI: http://dx.doi.org/10.15666/aeer/2305_1029310313

climate change. The ability of NDVI to reliably capture this sparse cover ensures more accurate monitoring of vegetation dynamics and ecosystem health across the entire landscape. Consequently, for large-scale ecological assessments and permafrost degradation studies reliant on UAV data upscaling within the QTP, NDVI emerges as the unequivocally preferred vegetation index.

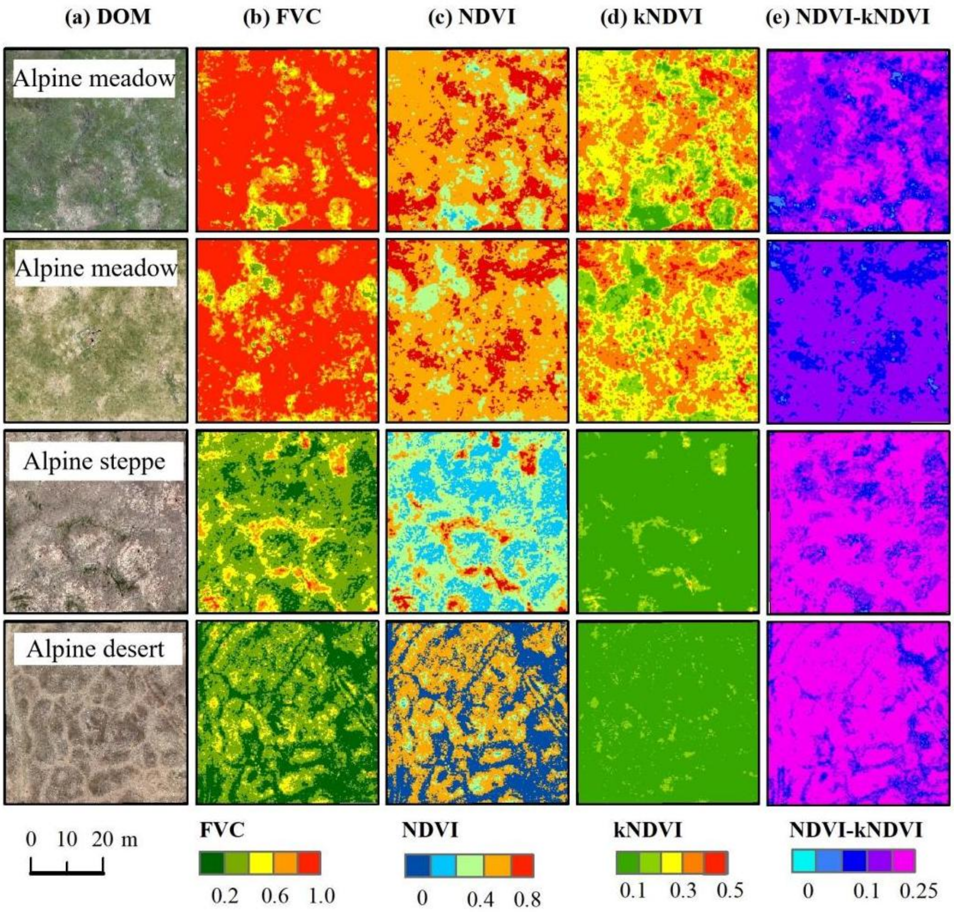

Figure 4. *Comparison of kernel normalized difference vegetation index (kNDVI) and normalized difference vegetation index (NDVI) in different alpine grassland types related to sub-grid heterogeneity*

Spatial pattern of vegetation characteristics revealed by UAV imagery

Based on the calibrated reflectance data from five multispectral bands of UAV, spatial distributions of NDVI, alpine grassland types, and FVC in the study area were derived (*Fig. 5*). As shown in *Figure 5a*, the NDVI values ranged from -0.62 to 0.93, with a mean NDVI of 0.21. Field validation demonstrates the classification accuracy, achieving an overall accuracy of 93.8% and a kappa coefficient of 0.925, indicating strong consistency between classification results and ground-truth data. Overall, at the kilometer scale, three alpine grassland types are identified: alpine meadow (39.0% of total area), alpine steppe (30.6%), and alpine desert (16.4%) (*Fig. 5b*). FVC exhibits maximum and minimum values of 0.96 and 0, respectively, with high-coverage areas (0.96) primarily distributed in alpine meadows and partial alpine steppe regions, while barren zones (0) predominantly occurred in alpine desert areas (*Fig. 5c*). Moreover, the

http://www.aloki.hu ● ISSN 1589 1623 (Print) ● ISSN 1785 0037 (Online)
DOI: http://dx.doi.org/10.15666/aeer/2305_1029310313

statistical analysis reveals distinct NDVI characteristics among vegetation types: alpine meadows exhibited the highest mean NDVI (0.62 ± 0.07), followed by alpine steppe (0.33 ± 0.05), while alpine desert showed a mean NDVI of 0.10 ± 0.02.

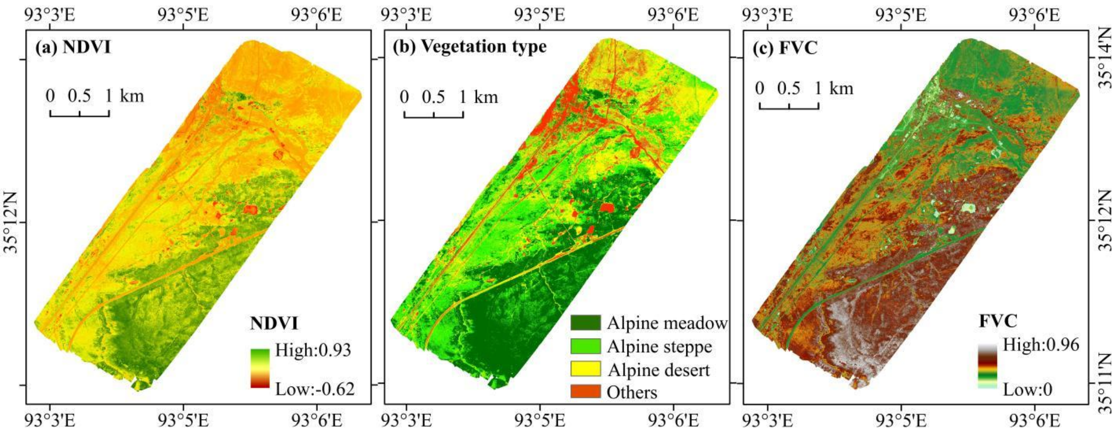

Figure 5. *The alpine grassland characteristics map of the study area: (a) the normalized difference vegetation index (NDVI) map; (b) the alpine grassland type map, and the fraction vegetation cover (FVC) map*

Discussion

Scaling bias in alpine grassland Fractional Vegetation Cover retrieval

Our fine-scale analysis of typical periglacial geomorphology (*Fig. 6*) reveals profound scaling biases in FVC retrieval driven by spatial resolution and surface heterogeneity. It can be found that, compared with the Sentinel-2 and Landsat-8 based FVC map, the submeter UAV imagery clearly resolves the heterogeneous patterns of alpine grassland FVC in the complex landforms of the permafrost region (e.g., Patterned ground, thaw gullies), which agree with Chen et al. (2016). Our fine-scale comparative analysis of periglacial geomorphology underscores the profound influence of spatial resolution and surface heterogeneity on the retrieval accuracy of alpine grassland FVC.

Compared to ground observations, UAV-based FVC retrieval results demonstrate the highest accuracy (>97%) across the five permafrost landforms, significantly outperforming Sentinel-2 (78%~85%) and Landsat OLI (61%~70%). The discrepancy stems from mixed pixels in satellite data, which amalgamate heterogeneous vegetation and bare soil signatures, particularly where microtopography creates sharp environmental gradients at sub-meter scales (Platel et al., 2025). As spatial resolution coarsens, separability between vegetation and background diminishes (Geng et al., 2022), leading to systematic underestimation of spatial heterogeneity—a critical limitation for monitoring vegetation dynamics in permafrost landscapes (Räsänen and Virtanen, 2018; Zhuo et al., 2024). Our findings align with Lin et al. (2021), demonstrating that detecting surface heterogeneity, not merely optimizing FVC parameters, is key to accuracy. Our findings align with Lin et al. (2021), demonstrating that detecting surface heterogeneity, not merely optimizing FVC parameters, is key to accuracy. Therefore, the neglect of vegetation heterogeneity may be the cause and consequence of the errors in vegetation change research in permafrost environment (Räsänen and Virtanen, 2018; Zhuo et al., 2024).

http://www.aloki.hu ● ISSN 1589 1623 (Print) ● ISSN 1785 0037 (Online)
DOI: http://dx.doi.org/10.15666/aeer/2305_1029310313

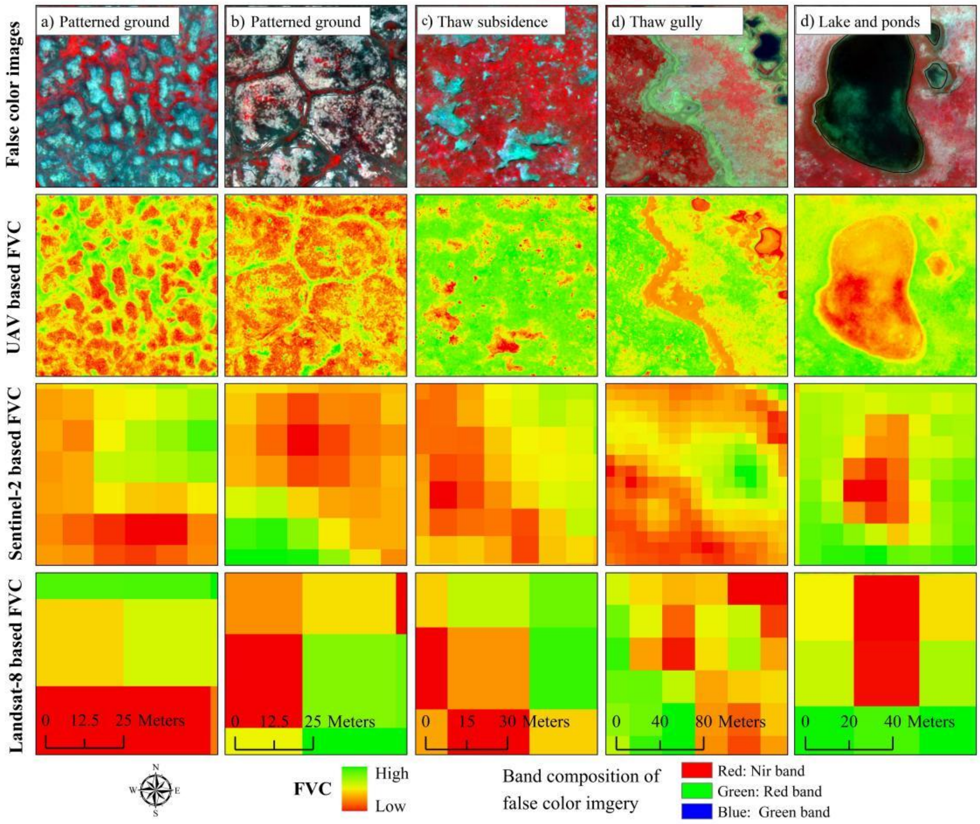

Figure 6. *Comparison of the fine-scale fraction vegetation cover (FVC) reflected by multiresolution remote sensing data in the typical periglacial geomorphology.*

Scaling bias in alpine grassland type classification

To evaluate the influence of sensor resolution on the classification of complex alpine vegetation communities within the periglacial environments, different resolution satellite datasets were used as the inputs of the SVM model. Specifically, Sentinel-2 MSI data, Landsat-8 OLI data, and Moderate Resolution Imaging Spectroradiometer (MODIS) surface reflectance data (230 m nominal resolution) were utilized. The resulting vegetation type classification maps are presented in *Figure 7*. A qualitative assessment reveals significant variations in classification fidelity directly attributable to spatial resolution. Overall, the vegetation type map generated from Sentinel-2 and Landsat-8 data was highly consistent with that generated using the UAV images. This superior performance is quantitively validated through pixel-by-pixel comparison with the UAV-derived map. Compared with the UAV-derived vegetation type map, the highest overlapping area (overlapping percentage of 84%) was achieved using Sentinel-2 MS data, followed by Landsat-8 MS data (overlapping percentage of 75%). While still indicating a reasonable level of accuracy for broader vegetation categories, the lower overlap reflects the inherent challenge of resolving finer vegetation patches and ecotones at this coarser resolution. The increased pixel size leads to a higher prevalence of mixed pixels, particularly along boundaries between distinct vegetation types, consequently reducing classification precision (Wang et al., 2022). The lowest classification accuracy was obtained using MODIS, particularly in the juncture of different vegetation types, where the uncertainty was higher.

http://www.aloki.hu ● ISSN 1589 1623 (Print) ● ISSN 1785 0037 (Online)
DOI: http://dx.doi.org/10.15666/aeer/2305_1029310313

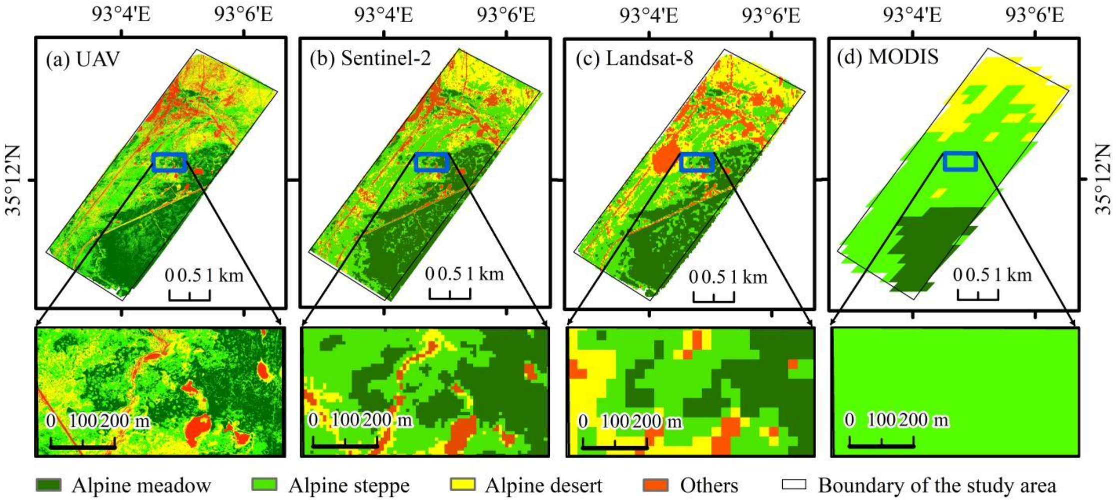

Figure 7. *Comparison of the alpine grassland type maps predicted using UAV and satellites: (a) UAV, (b) Sentinel-2, (c) Landsat-8, and (d) MODIS*

However, at the fine scale, we can conclude from the bottom data frame in *Figure 7* that the vegetation type was non-uniformly distributed across meter scale in the periglacial environments. For examples, polygonal patterned ground landscape, gully and river erosion, plateau pika holing activities, and the other thermokarst process, altered the vegetation types in the permafrost regions (Yang et al., 2021; Deng et al., 2022). Hence, we found that vegetation type was non-uniformly distributed across meter scale in the periglacial environments. The spatial disparities related to microtopography in vegetation types were neglected even in Sentinel-2 imagery. The details of spatial differences in vegetation type were neglected by satellite products. The results highlights that UAV-based photogrammetry enabled accurate subpixel heterogeneity detection of vegetation types in the periglacial environment of the QTP (Zhu et al., 2023). This capability is essential for reducing uncertainties in land surface models, where overlooking fine-scale vegetation transitions biases simulations of permafrost-vegetation-climate feedbacks.

Scaling bias of NDVI estimation

Besides of the influence of spatial resolution of remote sensing images on FVC and vegetation type retrieval, the accuracy of NDVI imagery represented a major source of retrieval error (Mu et al., 2024). In order to investigate the superiority of UAV-based NDVI data over heterogeneous underlying surfaces, a total of twelve Region of Interest (ROI) points were randomly selected, and it was ensured that each point and its searching radius were non-overlapping. We compared the UAV-based and satellite-based NDVI considering not only the value from a particular pixel but also the neighboring values in a certain buffer radius. Hence, five search radii, namely, 230 m, 460 m, 690 m, 920 m, and 1150 m, representing one, two, three, four, and five MODIS NDVI grid cells, respectively, were set for each ROI point. Then, the correlation and bias between the UAV- and satellite-based NDVI were calculated; the results are presented in *Figure 8*. The results show that the Sentinel-2 NDVI correlated strongly with UAV (mean $R = 0.78$, MBE = -0.04), followed by the Landsat-8. MODIS shows weak correlation and high bias. The correlation showed the largest value and the bias

http://www.aloki.hu ● ISSN 1589 1623 (Print) ● ISSN 1785 0037 (Online)
DOI: http://dx.doi.org/10.15666/aeer/2305_1029310313

showed the smallest value at a search radius of 690 m. Collectively, all satellites underestimated NDVI extreme (Max and Min), with MODIS exhibiting the largest error (MBE: -0.33 to -0.68). The correlation between the MODIS- and UAV-based NDVI increased and the bias decreased when the search radius was increased. However, the change trends become relatively stable after the buffering radius of 690 m. Therefore, the buffering radius of 690 m was used as the reference ROI size to further examine the scale effect on NDVI measurements. These results confirm that coarse resolutions misrepresent periglacial microtopography, flattening subgrid NDVI heterogeneity (Assmann et al., 2020).

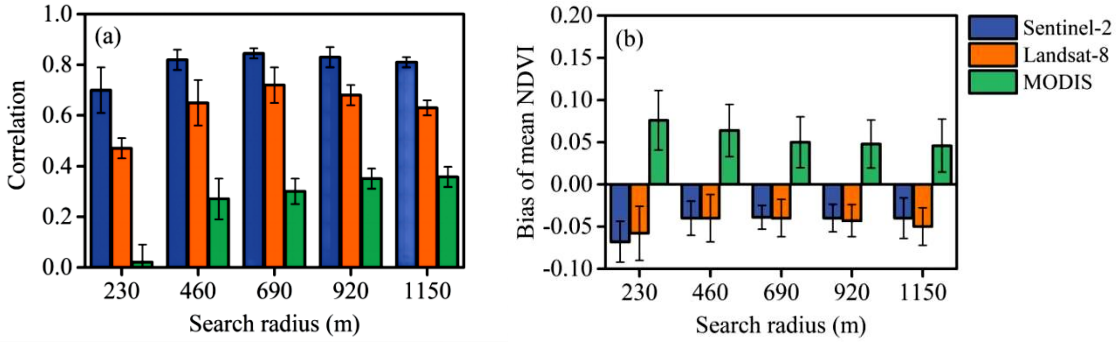

Figure 8. *Pearson's correlation testing and bias of UAV Normalized Difference Vegetation Index (NDVI) and different satellites data: (a) Pearson's correlation (n = 12), and (b) bias of UAV NDVI and three different satellites data (Sentinel-2, Landsat-8, and MODIS) with searching radii at 230 m, 460 m, 920 m, and 1150 m resolutions*

The detailed correlation metrics (R, MBE, RM, and RMSE) between the UAV and satellites in the twelve ROI regions with a 690 m radius were then calculated (*Fig. 9*). All statistics, including R, MBE, RM, and RMSE, show that a robust consistency is generated from the mean NDVI of Sentinel-2 and UAV, whereas the lowest consistency was from MODIS, which may be one of the most important causes for the underestimation associated with MODIS-derived vegetation growth for alpine vegetation (Fan and Bai, 2021). However, the highest error range appeared in the Max and Min NDVI of the three satellite datasets, with RM ranging from 0.40–0.49 and 0.3–0.69, respectively. Collectively, the satellite products underestimated subgrid NDVI heterogeneity (Max and Min), with MBEs ranging from -0.33 to -0.42 and -0.3 to -0.68, respectively. Overall, the correlation coefficient decreased and the error range increased as the sensor resolution increased owing to the misrepresentation of periglacial geomorphology and microtopography. The results highlight that UAV-based photogrammetry enabled accurate NDVI heterogeneity measurements of the vegetation at a high resolution (Zhuo et al., 2024). Although the Max and Min NDVI values cannot be well captured in medium and coarse-resolution satellite data, interestingly, even at a coarse-resolution scale, the mean NDVI had a high correspondence with UAV imagery.

Collectively, scaling biases arise from the decoupling between sensor resolution and characteristic scales of periglacial landform heterogeneity. Microtopographic create localized environmental gradients that govern vegetation distribution at scales finer than most satellite pixels (Lara et al., 2020; Song et al., 2022). When resolution coarsens, mixed pixels increase, eroding fine-grained ecological information.

http://www.aloki.hu ● ISSN 1589 1623 (Print) ● ISSN 1785 0037 (Online)
DOI: http://dx.doi.org/10.15666/aeer/2305_1029310313

Microtopography-driven vegetation patterns are homogenized. Retrieval accuracy declines nonlinearly. This has profound implications: scaling biases may propagate into land surface models, obscuring vegetation feedbacks on permafrost thaw (Li et al., 2024a). UAVs bridge the scale gap between field plots and satellites (Yue et al., 2021; Meng et al., 2022), enabling detection of processes invisible to satellites (Deng et al., 2022).

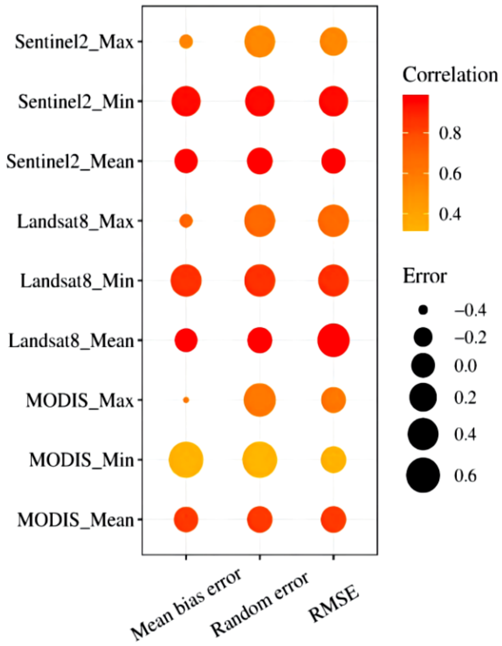

Figure 9. *Pearson's correlations of uncertainty metrics (mean bias error, random error, and RMSE, n = 12) and spatial attributes between UAV- and satellites-based Normalized Difference Vegetation Index (NDVI). The larger the bubble, the greater the error*

Limitations and future works

There are several sources of uncertainties in the data analysis that may affect the results. First, during the field campaign, although we considered the influence of the external experimental environment, such as wind speed, wind direction, precipitation, solar radiation, cloud cover, and flight stability, the harsh environment and changeable weather conditions hindered our field surveys, and sometimes, UAVs had to fly under suboptimal conditions. Thus, some uncertainties could have been introduced into UAV data and field measurements (Schaepman-Strub et al., 2006; Tan et al., 2020). The uncertainties were particularly significant in the high-altitude permafrost region of QTP (Liu et al., 2025).

To reduce the biases caused by the external experimental environment, we conducted rigorous radiometric and empirical calibrations and atmospheric correction. The error range of UAV spectral reflectance improved significantly after preprocessing and calibration. The analysis indicated that the linear regression method was a simple and effective method for calibrating UAV MS imagery (Guo et al., 2019). However, certain errors remained in UAV multispectral imaging. For example, during the UAV flight, a synchronous ground object spectrum was obtained using an ASD spectrometer. It was difficult to ensure that the solar elevation angle, zenith angle, and weather conditions

http://www.aloki.hu ● ISSN 1589 1623 (Print) ● ISSN 1785 0037 (Online)
DOI: http://dx.doi.org/10.15666/aeer/2305_1029310313

measured using ASD were consistent with those measured using the UAV owing to the cloudy and changeable weather conditions in the study area. Previous studies have also highlighted the challenges of radiometric consistency and repeatability when using multispectral drone sensors (Tu et al., 2018; Fischer et al., 2022), making high-quality UAV MS surveys on the QTP a challenging endeavor. Future studies should focus on exploiting more effective methods for radiometric calibration and atmospheric correction of the UAV imagery from specific areas (Suomalainen et al., 2021). Moreover, the field samples of ASD measurements in this study were insufficient for quantifying the relationship between spectral reflectance in in situ measurements and UAV imagery. Thus, more field surveys are necessary to improve the quality of UAV-based multispectral imagery.

Moreover, when comparing UAV and satellites NDVI data, several factors contribute to uncertainties, such as differences in acquisition periods, frequent cloud cover (Weng and Fu, 2014; Roy et al., 2014), inconsistent atmospheric correction and cloud screening procedures (Rumora et al., 2020), inconsistencies in the spatial/spectral resolutions of UAVs and satellite sensors (Alvarez-Vanhard et al., 2020), and the spectral characteristics of the sensor band center and bandwidth (Lin et al., 2021). The spatial misalignment of different remote sensing datasets and the measurements derived from them may also be a contributing factor (Berra et al., 2019). Although we aligned all datasets before comparison, some misalignment still occurred due to the "scale effect" between multiple remote sensing sources.

The changing ecosystems on the QTP requires an effective scale for the subgrid representation of heterogeneous landscapes and alpine grassland changes. The UAV technique fills the scale gap between the traditional satellites and field studies (Yue et al., 2021; Meng et al., 2022), allowing us to track the subpixel heterogeneity of alpine grasslands and their environmental factors. Despite mounting evidence indicating the occurrence of fine-scale microtopographic and landform-specific controls on ecosystems processes that govern ecosystems functions (Lara et al., 2018; Song et al., 2022), data limitations on the QTP have restricted our ability to understand the importance of scale-, process-, and landform-dependent responses to global change (Chen et al., 2022). This study provides deep insight into the subpixel spatial heterogeneity of vegetation in the periglacial environment. However, there are still limitations to this study.

Diverse periglacial landforms, including vegetation patches, thermo-erosion gullies, and thermokarst ponds and lakes, are distributed in the permafrost regions of the QTP (Heijmans et al., 2022; Aas et al., 2019; Nitzbon et al., 2020). However, the fine-scale vegetation patterns of each geomorphic type and their role in greening versus browning trends in the vegetation of the periglacial environment on the QTP are unclear (Deng et al., 2022). Thus, currently, a lack of understanding of the vegetation distribution disparities in the microtopography of permafrost regions is the greatest challenge in understanding the coupled relationship between climate, permafrost, and vegetation (Li et al., 2024b). Specifically, they guide the creation of flexible UAV-satellites integration approaches designed to enhance both spatial and temporal monitoring of vegetation in challenging environments (Hu et al., 2024; Li et al., 2024b). Furthermore, we recommend a wider investigation of the interaction process between vegetation, microtopography, and permafrost by combining field surveys, multitemporal UAV-based multisource imagery, high-resolution satellite data, and permafrost measurements.

http://www.aloki.hu ● ISSN 1589 1623 (Print) ● ISSN 1785 0037 (Online)
DOI: http://dx.doi.org/10.15666/aeer/2305_1029310313

Conclusions

This study substantiates that ignoring scale-dependent heterogeneity introduces systematic biases in alpine grassland monitoring. UAVs are not merely supplementary but essential for “ground-truthing” satellite retrievals in periglacial landscapes. Integrating multi-platform data across scales is imperative to unravel the complex interplay between vegetation, microtopography, and permafrost in a warming climate. By integrating field measurements, UAV data, and satellite products, we evaluated the accuracy of spectral reflectance, vegetation indices (VIs), fraction vegetation cover, and vegetation type classification, providing insights into scaling biases and optimal methodologies for alpine grassland monitoring. The main conclusions of this study are as follows:

(1) UAV-based surface reflectance calibration significantly improves the accuracy of spectral measurements across five bands (Blue, Green, Red, Red_edge, Nir), with mean R^2 increasing from 0.80 to 0.92 and RMSE decreasing from 0.05 to 0.03 after calibration. The ground-based spectral correction effectively minimized biases, enabling reliable retrieval of vegetation parameters. This highlights the necessity of calibration for UAV MS sensors to ensure data fidelity in high-altitude permafrost environments.

(2) Among five vegetation indices (NDVI, kNDVI, EVI, SAVI, ExG), NDVI exhibits superior performance in estimating fractional vegetation cover (FVC), achieving the highest correlation with field measurements ($R^2 = 0.980$, RMSE = 4.45%). While kNDVI showed comparable accuracy in densely vegetated areas, it failed to detect sparse vegetation, likely due to its nonlinear kernel function. NDVI’s robustness across all coverage levels, particularly in low-biomass alpine ecosystems, makes it the most suitable VI for FVC retrieval on the QTP, where sparse vegetation dominates.

(3) Vegetation type classification accuracy declines with coarser sensor resolutions. Sentinel-2 (10 m) achieved the highest overlap (83.7%) with UAV-derived maps, outperforming Landsat-8 (75.2%) and MODIS. However, even medium-resolution satellites overlooked fine-scale vegetation patterns linked to microtopography, such as polygonal patterned ground. This underscores UAV’s unique capability to resolve meter-scale heterogeneity driven by permafrost dynamics, thermokarst processes, and anthropogenic disturbances. For regional monitoring, integrating UAV data with Sentinel-2’s mean NDVI offers a balanced approach to capture both spatial detail and broad-scale trends.

These findings emphasize the critical role of UAVs in validating and enhancing satellites-derived vegetation products, particularly in complex periglacial landscapes where sub-grid heterogeneity challenges traditional remote sensing methods. Future work should focus on harmonizing multi-scale datasets to improve ecosystem models under climate change. Furthermore, we recommend a wider investigating the interaction process between the spectral and structural vegetation parameters with subsurface permafrost conditions.

Acknowledgments. This research was financially supported by the Soft Science Special Project of Gansu Basic Research Plan (24JRZA012), the Chinese Academy of Sciences “Light of West China” program (xbzg-zdsys-202304), Gansu Provincial Science and Technology Program (22ZD6FA005), the Program of the State Key Laboratory of Cryospheric Science and Frozen Soil Engineering, CAS (No. CSFSE-TZ-2402), the Innovation Fund Project of Colleges and Universities in Gansu Province (2025A-297), and the Project of Lanzhou Resources & Environment Voc-Tech University (X2023A-29).

REFERENCES

[1] Aas, K. S., Martin, L., Nitzbon, J., Langer, M., Boike, J., Lee, H., Berntsen, T. K., Westermann, S. (2019): Thaw processes in ice-rich permafrost landscapes represented with laterally coupled tiles in a land surface model. – Cryosphere 13(2): 591-609.

[2] Alvarez-Vanhard, E., Houet, T., Mony, C., Lecoq, L., Corpetti, T. (2020): Can UAVs fill the gap between in situ surveys and satellites for habitat mapping? – Remote Sensing of Environment 243: 111780.

[3] Assmann, J. J., Myers-Smith, I. H., Kerby, J. T., Cunliffe, A. M., Daskalova, G. N. (2020): Drone data reveal heterogeneity in tundra greenness and phenology not captured by satellites. – Environmental Research Letters 15(12): 125002.

[4] Berra, E. F., Gaulton, R., Barr, S. (2019): Assessing spring phenology of a temperate woodland: a multiscale comparison of ground, unmanned aerial vehicle and Landsat satellite observations. – Remote Sensing of Environment 223: 229-242.

[5] Biskaborn, B. K., Smith, S. L., Noetzli, J., Matthes, H., Vieira, G., Streletskiy, D. A., Schoeneich, P., Romanovsky, V. E., Lewkowicz, A. G., Abramov, A., Allard, M., Boike, J., Cable, W. L., Christiansen, H. H., Delaloye, R., Diekmann, B., Drozdov, D., Etzelmüller, B., Grosse, G., Guglielmin, M., Ingeman-Nielsen, T., Isaksen, K., Ishikawa, M., Johansson, M., Johannsson, H., Joo, H., Kaverin, D., Kholodov, A., Konstantinov, P., Kröger, T., Lambiel, C., Lanckman, J., Luo, D., Malkova, G., Meiklejohn, I., Moskalenko, N., Oliva, M., Phillips, M., Ramos, M., Sannel, A. B. K., Sergeev, D., Seybold, C., Skryabin, P., Vasiliev, A., Wu, Q., Yoshikawa, K., Zheleznyak, M., Lantuit, H. (2019): Permafrost is warming at a global scale. –Nature Communications 10(1): 264.

[6] Camps-Valls, G., Campos-Taberner, M., Moreno-Martínez, Á., Walther, S., Duveiller, G., Cescatti, A., Cescatti, A., Mahecha, M. D., Muñoz-Marí, J., García-Haro, F. J., Guanter, L., Jung, M., Gamon, J. A., Reichstein, M., Running, S. W. (2021): A unified vegetation index for quantifying the terrestrial biosphere. – Science Advances 7(9): eabc7447.

[7] Chen, A., Xu, C., Zhang, M., Guo, J., Xing, X., Yang, D., Xu, B., Yang, X. (2024): Cross-scale mapping of above-ground biomass and shrub dominance by integrating UAV and satellite data in temperate grassland. – Remote Sensing of Environment 304: 114024.

[8] Chen, J., Yi, S., Qin, Y., Wang, X. (2016): Improving estimates of fractional vegetation cover based on UAV in alpine grassland on the Qinghai–Tibetan Plateau. – International Journal of Remote Sensing 37(8): 1922-1936.

[9] Chen, J., Wu, T., Zou, D., Liu, L., Wu, X., Gong, W., Zhu, X., Li, R., Hao, J., Hu, G., Pang, Q., Zhang, J., Yang, S. (2022): Magnitudes and patterns of large-scale permafrost ground deformation revealed by Sentinel-1 InSAR on the central Qinghai-Tibet Plateau. – Remote Sensing of Environment 268: 112778.

[10] Deng, L., Mao, Z., Li, X., Hu, Z., Duan, F., Yan, Y. (2018): UAV-based multispectral remote sensing for precision agriculture: a comparison between different cameras. – ISPRS Journal of Photogrammetry and Remote Sensing 146: 124-136.

[11] Deng, Y., Li, X., Shi, F., Chai, L., Zhao, S., Ding, M., Liao, Q. (2022): Nonlinear effects of thermokarst lakes on peripheral vegetation greenness across the Qinghai-Tibet Plateau using stable isotopes and satellite detection. – Remote Sensing of Environment 280: 113215.

[12] Duan, H., Huang, B., Liu, S., Guo, J., Zhang, J. (2024): Impact of extreme climate indices on vegetation dynamics in the Qinghai–Tibet Plateau: a comprehensive analysis utilizing long-term dataset. – ISPRS International Journal of Geo-Information 13(12): 457.

[13] Fan, Z., Bai, X. (2021): Scenarios of potential vegetation distribution in the different gradient zones of Qinghai-Tibet Plateau under future climate change. – Science of the Total Environment 796: 148918.

[14] Fischer, R. L., Shuart, W. J., Anderson, J. E., Massaro, R. D., Ruby, J. G. (2022): Bidirectional reflectance distribution function modeling considerations in small

http://www.aloki.hu ● ISSN 1589 1623 (Print) ● ISSN 1785 0037 (Online)
DOI: http://dx.doi.org/10.15666/aeer/2305_1029310313

unmanned multispectral systems. – IEEE Journal of Selected Topics in Applied Earth Observations and Remote Sensing 15: 3564-3575.
[15] Ge, J., Meng, B., Liang, T., Feng, Q., Gao, J., Yang, S., Huang, X., Xie, H. (2018): Modeling alpine grassland cover based on MODIS data and support vector machine regression in the headwater region of the Huanghe River, China. –Remote Sensing of Environment 218: 162-173.
[16] Geng, X., Wang, X., Fang, H., Ye, J., Han, L., Gong, Y., Cai, D. (2022): Vegetation coverage of desert ecosystems in the Qinghai-Tibet Plateau is underestimated. – Ecological Indicators 137: 108780.
[17] Guo, Y., Senthilnath, J., Wu, W., Zhang, X., Zeng, Z., Huang, H. (2019): Radiometric calibration for multispectral camera of different imaging conditions mounted on a UAV platform. – Sustainability 11(4): 978.
[18] Gutman, G., Ignatov, A. (1998): The derivation of the green vegetation fraction from NOAA/AVHRR data for use in numerical weather prediction models. – International Journal of Remote Sensing 19(8): 1533-1543.
[19] Heijmans, M. M., Magnússon, R. Í., Lara, M. J., Frost, G. V., Myers-Smith, I. H., van Huissteden, J., Jorgenson, M. T., Fedorov, A. N., Epstein, H. E., Lawrence, D. M., Limpens, J. (2022): Tundra vegetation change and impacts on permafrost. – Nature Reviews Earth & Environment 3(1): 68-84.
[20] Holman, F. H., Riche, A. B., Castle, M., Wooster, M. J., Hawkesford, M. J. (2019): Radiometric calibration of 'commercial off the shelf' cameras for UAV-based high-resolution temporal crop phenotyping of reflectance and NDVI. – Remote Sensing 11(14): 1657.
[21] Hu, T., Cao, M., Zhao, X., Liu, X., Liu, Z., Liu, L., Huang, Z., Tao, S., Tang, Z., Guo, Y., Ji, C., Zheng, C., Wang, G., Hu, X., Zhou, L., Cheng, Y., Ma, W., Wang, Y., Zhang, P., Fan, Y., Su, Y. (2024): High-resolution mapping of grassland canopy cover in China through the integration of extensive drone imagery and satellite data. – ISPRS Journal of Photogrammetry and Remote Sensing 218: 69-83.
[22] Huete, A., Didan, K., Miura, T., Rodriguez, E. P., Gao, X., Ferreira, L. G. (2002): Overview of the radiometric and biophysical performance of the MODIS vegetation indices. – Remote Sensing of Environment 83(1-2): 195-213.
[23] Jin, X. Y., Jin, H. J., Iwahana, G., Marchenko, S. S., Luo, D. L., Li, X. Y., Liang, S. H. (2021): Impacts of climate-induced permafrost degradation on vegetation: a review. – Advances in Climate Change Research 12(1): 29-47.
[24] Kim, J., Kang, S., Seo, B., Narantsetseg, A., Han, Y. (2020): Estimating fractional green vegetation cover of Mongolian grasslands using digital camera images and MODIS satellite vegetation indices. – GIScience & Remote Sensing 57(1): 49-59.
[25] Lara, M. J., Nitze, I., Grosse, G., Martin, P., McGuire, A. D. (2018): Reduced arctic tundra productivity linked with landform and climate change interactions. – Scientific Reports 8(1): 2345.
[26] Lara, M. J., McGuire, A. D., Euskirchen, E. S., Genet, H., Yi, S., Rutter, R., Inersen, C., Sloan, V., Wullschleger, S. D. (2020): Local-scale Arctic tundra heterogeneity affects regional-scale carbon dynamics. – Nature Communications 11(1): 4925.
[27] Li, C., de Jong, R., Schmid, B., Wulf, H., Schaepman, M. E. (2020): Changes in grassland cover and in its spatial heterogeneity indicate degradation on the Qinghai-Tibetan Plateau. – Ecological Indicators 119: 106641.
[28] Li, H., Li, F., Xiao, J., Chen, J., Lin, K., Bao, G., Liu, A., Wei, G. (2024a): A machine learning scheme for estimating fine-resolution grassland aboveground biomass over China with Sentinel-1/2 satellite images. – Remote Sensing of Environment 311: 114317.
[29] Li, X., Li, X., Shi, Y., Zhao, S., Liu, J., Lin, Y., Li, C., Zhang, C. (2024b): Effects of microtopography on soil microbial communities in alpine meadows on the Qinghai-Tibetan Plateau. – Catena 239: 107945.

[30] Liljedahl, A. K., Witharana, C., Manos, E. (2024): The capillaries of the Arctic tundra. – Nature Water 2(7): 611-614.

[31] Lin, X., Chen, J., Lou, P., Yi, S., Qin, Y., You, H., Han, X. (2021): Improving the estimation of alpine grassland fractional vegetation cover using optimized algorithms and multi-dimensional features. – Plant Methods 17: 1-18.

[32] Liu, X., Qin, Y., Sun, Y., Yi, S. (2025): Monitoring Plateau Pika and revealing the associated influencing mechanisms in the alpine grasslands using unmanned aerial vehicles. – Drones 9(4): 298.

[33] Lou, P. (2022): Mapping permafrost thaw slumps with unmanned aerial vehicles. – Nature Reviews Earth & Environment 3(1): 4-4.

[34] Luo, L., Zhuang, Y., Zhang, M., Zhang, Z., Ma, W., Zhao, W., Zhao, L., Wang, L., Shi, Y., Zhang, Z., Duan, Q., Tian, D., Zhou, Q. (2020): An integrated observation dataset of the hydrological and thermal deformation in permafrost slopes and engineering infrastructure in the Qinghai–Tibet Engineering Corridor. – Earth System Science Data 13(8): 4035-4052.

[35] Marcial-Pablo, M. D. J., Ontiveros-Capurata, R. E., Jimenez-Jimenez, S. I., Ojeda-Bustamante, W. (2021): Maize crop coefficient estimation based on spectral vegetation indices and vegetation cover fraction derived from UAV-based multispectral images. – Agronomy 11(4): 668.

[36] Meng, Q., Intrieri, E., Raspini, F., Peng, Y., Liu, H., Casagli, N. (2022): Satellite-based interferometric monitoring of deformation characteristics and their relationship with internal hydrothermal structures of an earthflow in Zhimei, Yushu, Qinghai-Tibet Plateau. – Remote Sensing of Environment 273: 112987.

[37] Mu, C., Abbott, B. W., Norris, A. J., Mu, M., Fan, C., Chen, X., Jia, L., Yang, R., Zhang, T., Wang, K., Peng, X., Wu, Q., Guggenberger, G., Wu, X. (2020): The status and stability of permafrost carbon on the Tibetan Plateau. – Earth-Science Reviews 211: 103433.

[38] Mu, X., Yang, Y., Xu, H., Guo, Y., Lai, Y., McVicar, T. R., Xie, D., Yan, G. (2024): Improvement of NDVI mixture model for fractional vegetation cover estimation with consideration of shaded vegetation and soil components. – Remote Sensing of Environment 314: 114409.

[39] Nitzbon, J., Westermann, S., Langer, M., Martin, L. C., Strauss, J., Laboor, S., Boike, J. (2020): Fast response of cold ice-rich permafrost in northeast Siberia to a warming climate. – Nature Communication 11(1): 1-11.

[40] Nitzbon, J., Schneider von Deimling, T., Aliyeva, M., Chadburn, S. E., Grosse, G., Laboor, S., Lee, H., Lohmann, G., Steinert, N. J., Stuenzi, S. M., Werner, M., Westermann, S., Langer, M. (2024): No respite from permafrost-thaw impacts in the absence of a global tipping point. – Nature Climate Change 14(6): 573-585.

[41] Peng, X., Zhang, T., Frauenfeld, O. W., Wang, S., Qiao, L., Du, R., Mu, C. (2020): Northern Hemisphere greening in association with warming permafrost. – Journal of Geophysical Research: Biogeosciences 125(1): e2019JG005086.

[42] Pettorelli, N., Vik, J. O., Mysterud, A., Gaillard, J. M., Tucker, C. J., Stenseth, N. C. (2005): Using the satellite-derived NDVI to assess ecological responses to environmental change. – Trends in Ecology & Evolution 20(9): 503-510.

[43] Piao, S., Tan, J., Chen, A., Fu, Y. H., Ciais, P., Liu, Q., Janssens, I. A., Vicca, S., Zeng, Z., Jeong, S., Li, Y., Myneni, R. B., Peng, S., Shen, M., Peñuelas, J. (2015): Leaf onset in the northern hemisphere triggered by daytime temperature. – Nature Communications 6(1): 6911.

[44] Platel, A., Sandino, J., Shaw, J., Bollard, B., Gonzalez, F. (2025): Advancing sparse vegetation monitoring in the arctic and antarctic: a review of satellite and UAV remote sensing, machine learning, and sensor fusion. – Remote Sensing 17(9): 1513.

http://www.aloki.hu ● ISSN 1589 1623 (Print) ● ISSN 1785 0037 (Online)
DOI: http://dx.doi.org/10.15666/aeer/2305_1029310313

[45] Räsänen, A., Virtanen, T. (2019): Data and resolution requirements in mapping vegetation in spatially heterogeneous landscapes. – Remote Sensing of Environment 230: 111207.

[46] Ren, H., Zhou, G., Zhang, F. (2018): Using negative soil adjustment factor in soil-adjusted vegetation index (SAVI) for aboveground living biomass estimation in arid grasslands. – Remote Sensing of Environment 209: 439-445.

[47] Roy, D. P., Wulder, M. A., Loveland, T. R., Woodcock, C. E., Allen, R. G., Anderson, M. C., Helder, D., Irons, J. R., Johnson, D. M., Kennedy, R., Scambos, T. A., Schaaf, C. B., Schott, J. R., Sheng, Y., Vermote, E. F., Belward, A. S., Bindschadler, R., Cohen, W. B., Gao, F., Hipple, J. D., Zhu, Z. (2014): Landsat-8: Science and product vision for terrestrial global change research. – Remote Sensing of Environment 145: 154-172.

[48] Rumora, L., Miler, M., Medak, D. (2020): Impact of various atmospheric corrections on sentinel-2 land cover classification accuracy using machine learning classifiers. – ISPRS International Journal of Geo-Information 9(4): 277.

[49] Schaepman-Strub, G., Schaepman, M. E., Painter, T. H., Dangel, S., Martonchik, J. V. (2006): Reflectance quantities in optical remote sensing—definitions and case studies. – Remote Sensing of Environment 103(1): 27-42.

[50] Song, W., Mu, X., McVicar, T. R., Knyazikhin, Y., Liu, X., Wang, L., Niu, Z., Yan, G. (2022): Global quasi-daily fractional vegetation cover estimated from the DSCOVR EPIC directional hotspot dataset. –Remote Sensing of Environment 269: 112835.

[51] Suomalainen, J., Oliveira, R. A., Hakala, T., Koivumäki, N., Markelin, L., Näsi, R., Honkavaara, E. (2021): Direct reflectance transformation methodology for drone-based hyperspectral imaging. –Remote Sensing of Environment 266: 112691.

[52] Tan, K., Niu, C., Jia, X., Ou, D., Chen, Y., Lei, S. (2020): Complete and accurate data correction for seamless mosaicking of airborne hyperspectral images: a case study at a mining site in Inner Mongolia, China. –ISPRS Journal of Photogrammetry and Remote Sensing 165: 1-15.

[53] Tu, Y. H., Phinn, S., Johansen, K., Robson, A. (2018): Assessing radiometric correction approaches for multi-spectral UAS imagery for horticultural applications. – Remote Sensing 10(11): 1684.

[54] Wang, H., Liu, H., Huang, N., Bi, J., Ma, X., Ma, Z., Shangguan, Z., Zhao, H., Feng, Q., Liang, T., Cao, G., Schmid, B., He, J. (2021a): Satellite-derived NDVI underestimates the advancement of alpine vegetation growth over the past three decades. – Ecology e03518.

[55] Wang, R., Gamon, J. A., Moore, R., Zygielbaum, A. I., Arkebauer, T. J., Perk, R., Leavitt, B., Cogliati, S., Waedlow, B., Qi, Y. (2021b): Errors associated with atmospheric correction methods for airborne imaging spectroscopy: implications for vegetation indices and plant traits. – Remote Sensing of Environment 265: 112663.

[56] Wang, Y., Lv, W., Xue, K., Wang, S., Zhang, L., Hu, R., Zeng, H., Xu, X., Li, Y., Jiang, L., Hao, J., Du, J., Sun, J., Doeji, T., Piao, S., Wang, C., Luo, C., Zhang, Z., Chang, X., Zhang, M., Hu, Y., Wu, T., Wang, J., Li, B., Liu, P., Zhou, Y., Wang, A., Dong, S., Zhang, X., Gao, Q., Zhou, H., Shen, M., Wilkes, A., Miehe, G., Zhao, X., Niu, H. (2022): Grassland changes and adaptive management on the Qinghai–Tibetan Plateau. – Nature Reviews Earth & Environment 3(10): 668-683.

[57] Wang, Z., Wang, Q., Zhao, L., Wu, X., Yue, G. Y., Zou, D., Nan, Z., Liu, G., Pang, Q., Fang, H., Wu, T., Shi, J., Jiao, K., Zhao, Y., Zhang, L. (2016): Mapping the vegetation distribution of the permafrost zone on the Qinghai-Tibet Plateau. – Journal of Mountain Science 13: 1035-1046.

[58] Wen, A., Wu, T., Zhu, X., Chen, J., Shi, J., Lou, P., Wang, D., Ma, X., Wu, X. (2025): Evaluation of the Geomorphon approach for extracting troughs in polygonal patterned ground across different permafrost environments. – Remote Sensing 17(6): 1040.

[59] Weng, Q., Fu, P. (2014): Modeling annual parameters of clear-sky land surface temperature variations and evaluating the impact of cloud cover using time series of Landsat TIR data. – Remote Sensing of Environment 140: 267-278.

http://www.aloki.hu ● ISSN 1589 1623 (Print) ● ISSN 1785 0037 (Online)
DOI: http://dx.doi.org/10.15666/aeer/2305_1029310313

[60] Woebbecke, D. M., Meyer, G. E., Von Bargen, K., Mortensen, D. A. (1995): Color indices for weed identification under various soil, residue, and lighting conditions. – Transactions of the ASAE 38(1): 259-269.
[61] Yang, D., Morrison, B. D., Hantson, W., Breen, A. L., McMahon, A., Li, Q., Salmon, V. G., Hayers, D. J., Serbin, S. P. (2021): Landscape-scale characterization of Arctic tundra vegetation composition, structure, and function with a multi-sensor unoccupied aerial system. – Environmental Research Letters 16(8): 085005.
[62] Yang, Y., Wang, X., Wang, T. (2024): Permafrost degradation induces the abrupt changes of vegetation NDVI in the Northern Hemisphere. – Earth's Future 12(10): e2023EF004309.
[63] Yi, S., Iwahana, G., Qin, Y., Sun, Y. (2021): Applications of UAVs in cold region ecological and environmental studies. – Remote Sensing 13(13): 2472.
[64] Yue, J., Guo, W., Yang, G., Zhou, C., Feng, H., Qiao, H. (2021): Method for accurate multi-growth-stage estimation of fractional vegetation cover using unmanned aerial vehicle remote sensing. – Plant Methods 17(1): 51.
[65] Zhang, H., Tang, Z., Wang, B., Meng, B., Qin, Y., Sun, Y., Lv, Y., Zhang, J., Yi, S. (2022): A non-destructive method for rapid acquisition of grassland aboveground biomass for satellite ground verification using UAV RGB images. – Global Ecology and Conservation 33: e01999.
[66] Zhong, G., Chen, J., Huang, R., Yi, S., Qin, Y., You, H., Han, X., Zhou, G. (2023): High spatial resolution fractional vegetation coverage inversion based on UAV and Sentinel-2 data: a case study of alpine grassland. – Remote Sensing 15(17): 4266.
[67] Zhou, G., Ren, H., Zhang, L., Lv, X., Zhou, M. (2025): Annual vegetation maps in the Qinghai–Tibet Plateau (QTP) from 2000 to 2022 based on MODIS series satellite imagery. – Earth System Science Data 17(2): 773-797.
[68] Zhu, Q., Chen, H., Peng, C., Liu, J., Piao, S., He, J., Wang, S., Zhao, X., Zhang, J., Fang, X., Jin, J., Yang, Q., Ren, Li., Wang, Y. (2023): An early warning signal for grassland degradation on the Qinghai-Tibetan Plateau. – Nature Communications 14(1): 6406.
[69] Zhu, X., Wu, T., Chen, J., Wu, X., Wang, P., Zou, D., Yue, G., Yan, X., Ma., Wang, D., Lou, P., Wen, A., Shang, C., Liu, W. (2024): Summer heat wave in 2022 led to rapid warming of permafrost in the central Qinghai-Tibet Plateau. – NPJ Climate and Atmospheric Science 7(1): 216.
[70] Zhuo, W., Wu, N., Shi, R., Liu, P., Zhang, C., Fu, X., Cui, Y. (2024): Aboveground biomass retrieval of wetland vegetation at the species level using UAV hyperspectral imagery and machine learning. – Ecological Indicators 166: 112365.

http://www.aloki.hu ● ISSN 1589 1623 (Print) ● ISSN 1785 0037 (Online)
DOI: http://dx.doi.org/10.15666/aeer/2305_1029310313